16

Ganymede's Tenuous Atmosphere

LORENZ ROTH, CHRISTINA PLAINAKI, APURVA V. OZA, AUDREY VORBURGER, ROBERT E. JOHNSON, PHILIPPA M. MOLYNEUX, KURT D. RETHERFORD, FRANÇOIS LEBLANC, STEFANO MASSETTI, ALESSANDRO MURA, AND PETER WURZ

16.1 INTRODUCTION

Years before a definitive detection of neutral gas abundance around Ganymede, studies suggested that an atmosphere consisting of water group species could be produced from sublimation. Based on an early but eventually incorrect detection of a significant atmosphere (Carlson et al., 1973), Yung and McElroy (1977) suggested that a significant atmosphere could be present, produced by photochemistry in a sublimated water vapor. Such an atmosphere would be dominated by O_2, which is gravitationally bound but does not recondense on the surface. During the Voyager 1 flyby, it was found that the plasma trapped in the Jovian magnetosphere was more intense and had a different composition than predicted.[1] This led a group at Bell Labs to carry out a series of experiments which showed that the icy satellite surfaces would be significantly eroded by the incident plasma ions (Lanzerotti et al., 1978). They called this process 'electronic sputtering' as, although it appeared to be related to a standard laboratory process for directly knocking atoms from a solid into the gas phase (called 'nuclear sputtering'), it was much more efficient and was a result of the electronic excitations produced in ice by the incident ions (Brown et al., 1978). The Voyager plasma ion flux combined with the laboratory measurements were used to show that, depending on the local surface temperature, the sputter production of gas phase species could dominate sublimation (Johnson et al., 1981). It was subsequently shown that the species ejected primarily consisted of H_2O, O_2, and H_2 with only small fractions of dissociation products (Brown et al., 1982). Because H_2 most easily escapes from the moons and H_2O readily condenses, O_2 is indeed likely to be the dominant atmospheric component over most of the icy satellite surfaces due to its gravitational confinement and the fact that it is directly produced from the surface (Johnson et al., 1981) rather than by photochemistry in a tenuous atmosphere (Yung and McElroy, 1977).

In this chapter we review the observational and theoretical studies related to Ganymede's atmosphere. An earlier review can be found in McGrath et al. (2004) but there have been crucial new insights and results since then, like the recent detection of H_2O. The chapter is structured as follows: Section 16.2 summarizes the observational studies. In Section 16.3, we elaborate on the role of the sources and sinks for Ganymede's atmosphere. Section 16.4 describes the various theoretical and modelling studies and their contributions to today's understanding. Finally, in Section 16.5, we summarize the current knowledge and open questions on Ganymede's atmosphere and describe the prospects and plans of the upcoming Jupiter ICy moons Explorer (JUICE) mission.

We also want to point to the most relevant related chapters in this book. Surface erosion processes and their role in constantly sustaining the atmosphere are discussed in Chapter 15. The ionosphere and how it is formed from the atmosphere through different ionization processes are described in Chapter 17. Both atmosphere and ionosphere are also crucial for the interaction of Ganymede and its magnetic field with the surrounding Jovian magnetosphere, presented in Chapter 14. Finally, Ganymede's aurora (Chapter 18) is closely related to the atmosphere, not only through the physical processes but also because observations of the electron-excited aurora are the primary evidence for the moon's bound atmosphere.

16.2 OBSERVATIONS

In this section we discuss the observational constraints on Ganymede's atmosphere. While there are observational means to indirectly constrain the neutral gas abundance in Ganymede's environment, for example, through plasma observations and simulations of the atmosphere–plasma interaction, the focus here will be on the direct detection of neutral species. Table 16.1 summarizes all observations of Ganymede's neutral atmosphere since the first detections and provides details on the instruments and set-ups.

16.2.1 Early Constraints

In their search for an atmosphere, Carlson et al. (1973) observed an occultation of a star (SAO 186800) by Ganymede from three locations in India, Java and Australia. The authors found a gradual increase above Ganymede's disk in the transit light curve and concluded that an atmosphere with surface pressure around 1 μbar was present on Ganymede (Carlson et al., 1973; Taylor, 1971). No atmospheric signature was found on Io in a similar observation, and the authors concluded that Ganymede's atmosphere should be denser than Io's (Taylor, 1971).

Almost a decade later, an occultation measurement by the Ultraviolet Spectrometer (UVS) on board the Voyager 1 spacecraft of the brighter star κ Centauri by Ganymede provided higher sensitivity, but no signatures of atmospheric absorption

[1] By 'plasma' we refer to charged particles of all energies throughout this chapter (including, e.g., keV and MeV ions).

https://doi.org/10.1017/9781108966474.017 Published online by Cambridge University Press

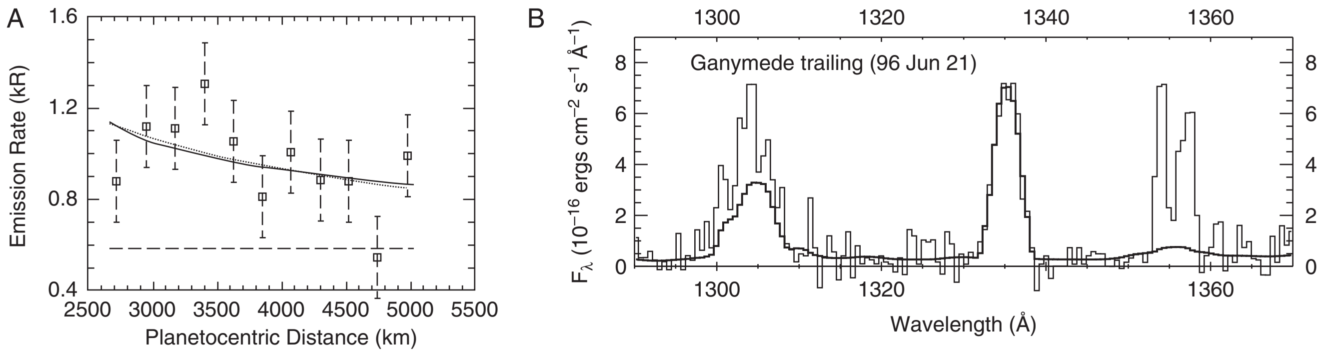

Figure 16.1 (a) First detection of Ganymede's H corona in observations of HI Lyman-α emissions above Ganymede's limb taken by Galileo UVS adapted from *Geophysical Research Letters*, 24(17), C. A. Barth, C. W. Hord, A. I. F. Stewart, W. R. Pryor, K. E. Simmons, W. E. McClintock, J. M. Ajello, K. L. Naviaux, J. J. Aiello. Galileo ultraviolet spectrometer observations of atomic hydrogen in the atmosphere of Ganymede, 185–198., ©1997, with permission from John Wiley and Sons. (b) First detection of Ganymede's bulk molecular atmosphere through emissions at the oxygen multiplets at 1304 Å and 1356 Å in a HST/GHRS spectrum (adapted from Hall et al., 1998, figure 1). The CII 1335 Å feature is used to adjust the surface-reflected solar spectrum.

were found (Broadfoot et al., 1981). A density upper limit of 1.5×10^9 cm^{-3} at the surface was inferred for a O_2 or H_2O atmosphere, which would convert to a column density of about 10^{16} cm^{-2}. This corresponds to a surface pressure of 2×10^{-5} μbar, almost five orders of magnitude lower than, and thus incompatible with, the value from Carlson et al. (1973). Later observations confirmed the tenuous nature of Ganymede's atmosphere, and the Voyager UVS upper limit still holds today.

16.2.2 First Detection of H Corona and Later Confirmations

The first positive detection of a neutral species around Ganymede was achieved by the ultraviolet spectrometer (UVS) on board the Galileo spacecraft in 1996. The spectrometer detected slowly decreasing H Lyman-α emissions in a scan from Ganymede's surface to 5 000 km altitude (Barth et al., 1997) (Figure 16.1a). The gradual emission profile and overall intensity were shown to be consistent with an extended corona of atomic hydrogen with maximum density at the surface of 1.5×10^4 cm^{-3}. The H abundance was suggested to originate from water vapor (H_2O) in the atmosphere (Barth et al., 1997).

Confirmation of extended H Lyman-α emissions around Ganymede and thus the presence of the H corona was provided by observations by the Space Telescope Imaging Spectrograph of the Hubble Space Telescope (HST/STIS) taken in 1998 (Feldman et al., 2000). The STIS was used in imaging spectroscopy mode, providing spatially resolved images at various wavelengths including hydrogen Lyman-α line and two far-UV oxygen multiplets. This STIS observation mode provided a series of important insights on Ganymede (cf. Sections 16.2.3 and 16.2.4) and was employed in several later observing campaigns (Table 16.1).

Alday et al. (2017) analyzed the extended H Lyman-α emissions in all HST/STIS observations taken between 1998 and 2014 (Table 16.1). Taking into account various contributions to the signal such as surface reflections scattered off the limb, they found a relatively stable H corona with surface densities in the range of $(5–8)\times10^3$ cm^{-3}. Systematic differences, for example between leading or trailing hemisphere or temporal changes, could not be identified. Alday et al. (2017) suggest that the H is produced in the atmosphere through dissociation of both H_2O (as first suggested by Barth et al. (1997)) and H_2, referring to the simulations from Marconi (2007).

16.2.3 Hubble Space Telescope Observations I: Atmospheric Oxygen Emissions

Far-UV atomic oxygen emissions near 1 304 Å and 1 356 Å from Ganymede's atmosphere were observed for the first time in a spectrum taken by the Goddard High Resolution Spectrograph of the Hubble Space Telescope (HST/GHRS) observing the moon's trailing hemisphere (Hall et al., 1998); see Figure 16.1b.

The relative brightness of the emissions from the spin-forbidden OI(^{5}S–^{3}P) 1 356 Å doublet and the optically allowed OI(^{3}S–^{3}P) 1 304 Å triplet was used as diagnostic of the excitation process. The derived OI 1356 Å/OI 1 304 Å oxygen ratio ($r_{\gamma O}$) of 1.3±0.3 was interpreted to relate to dissociative excitation of O_2 by electrons. The reasoning is that electron-impact excitation processes that involve other possible species in the atmosphere such as O or H_2O produce significantly brighter 1 304 Å emissions ($r_{\gamma O} < 1$). In addition, resonant scattering of solar emissions by atomic oxygen O contributes to the OI 1 304 Å brightness, but is absent at 1 356 Å (Hall et al., 1995). Electron-impact excitation of O_2 results in a larger OI 1 356 Å/OI 1 304 Å ratio of $r_{\gamma O} > 2.2$.

Figure 16.2 shows calculated excitation rates for a range of possible electron temperatures based on the laboratory cross sections and a schematic illustrating approximate oxygen emission ratios related to different constituents. The use of the oxygen ratio as diagnostic is further discussed in Section 16.2.4.

Before the detection at Ganymede, HST/GHRS observations had revealed oxygen FUV emissions at Europa, also with higher intensity at 1 356 Å than at 1 304 Å. The same diagnostic was used to derive O_2 in the atmosphere of Europa (Hall et al., 1995). Later on, the Cosmic Origins Spectrograph (COS), installed on HST in 2009, detected faint oxygen emissions also from Callisto, thanks to its superior sensitivity. The higher OI 1 356 Å intensity was again interpreted as originating from an O_2-dominated atmosphere (Cunningham et al., 2015).

The double-peak structure of the oxygen emissions in the GHRS spectrum on Ganymede (Figure 16.1, particularly at 1 356 Å) pointed to a non-uniform spatial distribution and was

https://doi.org/10.1017/9781108966474.017 Published online by Cambridge University Press

Table 16.1 *Observations of Ganymede's neutral atmosphere and corona*

Facility/ program ID	Instrument	Year	Geometry/ hemisphere	Type	Comments	Ref.
Galileo	UVS	1996	above limb	FUV spectral scan	first detection of H through scattered solar Lyα	[a]
HST 6758	GHRS	1996	trailing	FUV spectrum	first detection of O_2	[b]
HST 7939	STIS	1998	trailing	spectral images	detection of auroral bands & of H_2O	[c,d,f,g,j]
HST 8224	STIS	2000	leading	spectral images	first images of leading hemisphere	[d,f,g]
HST 9296	STIS	2003	sub-Jovian	spectral images	first images of sub-Jovian hemisphere	[d]
New Horizons	Alice	2007	sub- & anti-Jovian	FUV spectra	observation of nightside atmosphere	Section 16.2.5
HST 10871	ACS	2007	sub-Jovian	FUV filter image	observation in eclipse	[d]
HST 12244	STIS	2010/11	leading	spectral images	temporal variability, H_2O	[e,f,g,j]
Herschel	HIFI	2011–13	leading & trailing	sub-mm spectrum	possible detection of H_2O absorption	[i]
HST 13328	STIS & COS	2014	leading & trailing	spectra & spectral images	first campaign to observe both hemispheres	[f,h]
HST 14634	STIS	2017	anti-Jovian	spectral images	first images of anti-Jovian hemisphere	
	COS	2018	sub-Jovian	high-res spectra	eclipse/egress observation/upper limits on O	[j]

[a]Barth et al. (1997), [b]Hall et al. (1998),[c]Feldman et al. (2000), [d]McGrath et al. (2013), [e]Saur et al. (2015), [f]Alday et al. (2017), [g]Musacchio et al. (2017), [h]Molyneux et al. (2018), [i]Hartogh et al. (2013), [j]Roth et al. (2021).

shown to be consistent with the emissions being confined to the polar regions (Hall et al., 1998). The first observations with HST/STIS in imaging spectroscopy mode from 1998 then provided confirmation that the oxygen OI 1 356 Å emissions on Ganymede's trailing hemisphere are indeed brightest near the north and south poles. Further STIS images of the orbital-leading and sub-Jovian hemispheres showed that the regions of brightest OI 1 356 Å emissions are roughly colocated with the open-closed-field-line-boundary (OCFB) of Ganymede's mini-magnetosphere (McGrath et al., 2013). The emission morphology is thus determined by the magnetic field topology and by the precipitation patterns of the electrons that excite the emissions in the atmosphere (see Chapter 17 for more details). Furthermore, Eviatar et al. (2001) showed that electrons must be accelerated to produce the observed intensities, but the acceleration mechanism and exact energies are unknown.

The auroral nature and particular morphology of the oxygen emissions enabled studies of various magnetospheric and plasma processes (Chapter 18; Saur et al., 2015; Musacchio et al., 2017). However, the derivation of neutral gas abundances from the electron-excited oxygen emissions is difficult given the uncertainty of the electron properties at the OCFB or inside and around Ganymede's magnetosphere. The first approximations assumed a homogeneous plasma with constant electron temperature and density to derive a line-of-sight O_2 column density averaged over the moon's disk around 10^{14} cm^{-2} to 10^{15} cm^{-2} (Hall et al., 1998; Feldman et al., 2000). Using the ionosphere model of Eviatar, Vasyliūnas and Gurnett (2001), Eviatar et al. (2001) found that electrons need to be accelerated locally such that some sub-population attains energies (temperatures) in the range of 75–300 eV to effectively produce the observed intensities with an atmosphere of $\sim 3\times10^{14}$ O_2 cm^{-2}.

These global column densities are derived from average intensities over the disk and neglect the spatial variations and peak intensities. In the case of Europa, the oxygen emissions are less confined to specific regions and are possibly excited by the thermal electron population in the plasma sheet (Hall et al., 1995; Saur et al., 1998; Roth et al., 2016). For this thermal population, estimates of density and temperature were made based on spacecraft measurements near Europa's orbit (Bagenal et al., 2015; Bagenal and Dols, 2020). There, the simplifying approach of relating a globally averaged intensity to a disk-average column density is probably more justified than in the

https://doi.org/10.1017/9781108966474.017 Published online by Cambridge University Press

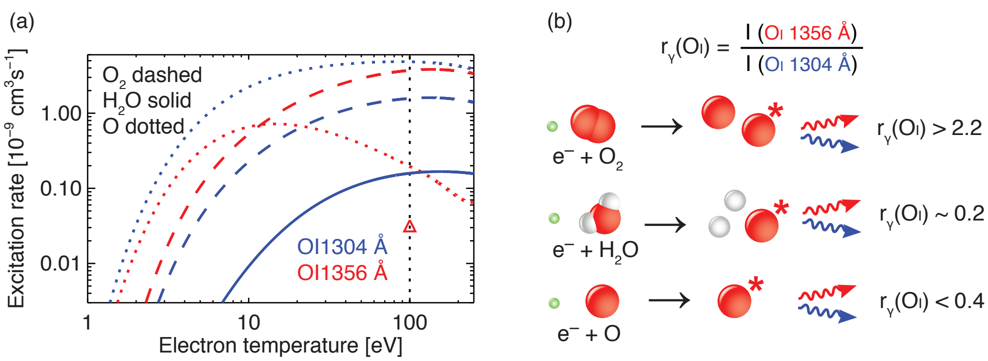

Figure 16.2 (a) Excitation rates for electron impact on O_2 (dashed), O (dotted) and H_2O (solid) for OI 1 356 Å (red) and OI 1 304 Å (blue) as a function of electron temperature. The rates are calculated from the cross sections (Kanik et al., 2001, 2003; Makarov et al., 2004), assuming Maxwellian temperature distribution for the electron population. For OI 1 356 Å from H_2O only a single cross-section measurement at 100 eV is available, and the red triangle (for the OI 1 356 Å rate) shows the 1 304 Å value scaled according to the relative cross section. (b) Schematic showing the approximate oxygen emission ratios for the three species (after Roth et al., 2021).

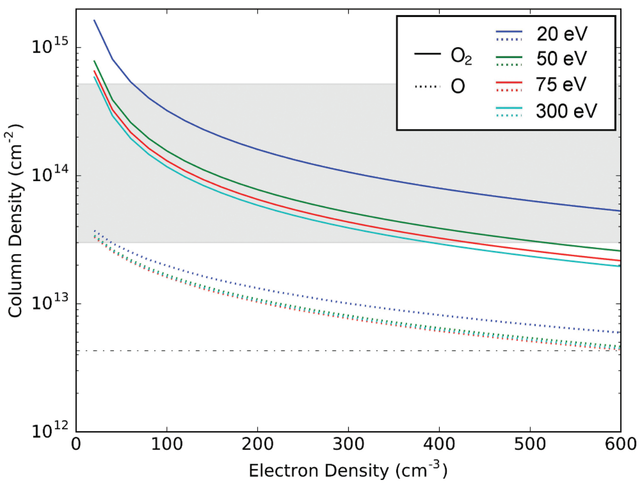

Figure 16.3 Global column densities of O_2 and O at Ganymede based on the oxygen emission intensities observed on the trailing hemisphere for a range of electron densities and temperatures. The O_2 column density is primarily constrained by a disk-average 1 356 Å intensity of 39 R, derived in Molyneux et al. (2018). The shaded region shows the range of O_2 column densities inferred from previous observations of Ganymede (Feldman et al., 2000). The dashed horizontal line indicates the maximum column density for an optically thin O atmosphere at a temperature of 150 K.

case of Ganymede, where the system is likely highly dynamic and electron density and temperature can assume a wide range. Figure 16.3 shows the required column densities to explain the intensities observed by Molyneux et al. (2018) as a function of electron density for different electron temperatures, again assuming a homogeneous plasma environment.

If the atmospheric temperatures T are in the range of the surface temperatures of 80 K to 150 K (Orton et al., 1996), the nominal atmospheric scale height for O_2 is about 20 km. Assuming the actual effective atmospheric scale height of O_2 is between 10 km and 100 km, the estimated average O_2 column densities (10^{14} cm^{-2} to 10^{15} cm^{-2}) correspond to surface densities of 10^7 to 10^9 cm^{-3}. This is below, and thus consistent with, the upper limit on the molecular atmosphere from the Voyager UVS (Broadfoot et al., 1981).

16.2.4 Hubble Space Telescope Observations II: Oxygen Emission Ratio Studies

Hubble Space Telescope observations of Ganymede generally have a lower signal-to-noise ratio at 1 304 Å than at 1 356 Å because Ganymede's atmospheric OI 1 304 Å emissions have a lower intensity, while the background signal is higher due to both higher solar flux (leading to increased background from surface reflection) and an additional contribution from the Earth's geocorona at 1 304 Å. Therefore, most studies of the oxygen emissions and their morphology used primarily the 1 356 Å aurora. However, the relative intensity of the OI 1 304 Å to the OI 1 356 Å emissions (or the OI 1 356 Å/OI 1 304 Å ratio, $r_{\gamma O}$) can provide insights into both atmospheric and plasma processes. The ratio is widely different for different species such as O_2, H_2O or O, but also varies with the temperature of the exciting electrons as shown in Figure 16.2. Excitation of atomic oxygen is the most effective process at low temperatures ($T_e <$ 5 eV) and produces significantly more OI 1 304 Å emission. For electron temperatures near and above the O_2 dissociation threshold (roughly $T_e >$ 10 eV), excitation of O_2 becomes similarly efficient but produces more 1 356 Å emission. Dissociative excitation of H_2O has overall lower rates for producing oxygen emission, thus requiring larger abundances to reach similar intensities. A single measurement of the OI 1356 Å yield from impact of 100-eV electrons suggests a OI 1 356 Å/OI 1 304 Å ratio of $r_{\gamma O} \sim 0.2$ from H_2O.

The OI 1 356 Å/OI 1 304 Å ratio derived from earlier GHRS and STIS data revealed ratios between 1.2 and 3.2 (with large uncertainties), most consistent with an O_2 atmosphere (Hall et al., 1998; Feldman et al., 2000).

The first observations of Ganymede using HST's high-sensitivity Cosmic Origins Spectrograph (COS) and of both the leading and trailing hemispheres within a single HST campaign then revealed a systematic difference in the OI 1 356 Å/OI 1 304 Å ratio between the two hemispheres (Molyneux et al., 2018). On the sunlit leading side, the ratio of the globally average intensities was found to be $r_{\gamma O} = 2.7 \pm 0.5$, thus even larger than, but still consistent with, pure O_2 within uncertainty. The average ratio found for the sunlit trailing side of $r_{\gamma O} = 1.4 \pm 0.2$ was significantly lower, requiring a constituent other than O_2 to reduce $r_{\gamma O}$ to values below 2 (Figure 16.2b). Assuming this

https://doi.org/10.1017/9781108966474.017 Published online by Cambridge University Press

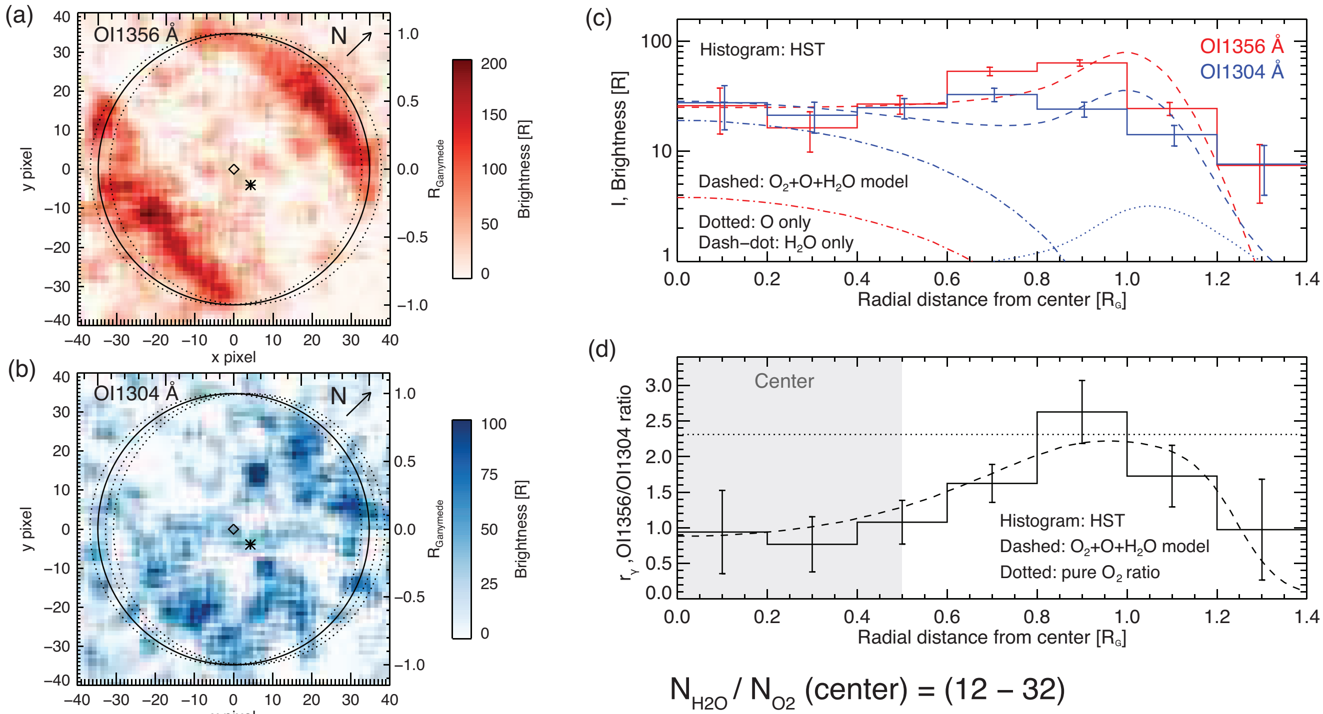

Figure 16.4 (a) and (b) HST/STIS images of the OI 1 356 Å and OI 1 304 Å emissions observing Ganymede's trailing hemisphere from Roth et al. (2021) (see their figure 3 for more details). (c) The radial brightness profiles derived from these OI 1 356 Å (red) and OI 1 304 Å (blue) images show that near the disk centre both emissions reach similar intensities. Simulated radial profiles for an assumed H_2O-O_2-O atmosphere model are shown for the total modelled intensity (dashed) and for individual contributions. (e) The profile of the observed oxygen emission ratio $r_\gamma(\mathrm{OI})$ agrees with the ratio of O_2 (dotted) only near the limb but is in good agreement with the O_2+O+H_2O atmosphere model (dashed) assumed by Roth et al. (2021) at all radial distances. The derived column density ratio N_{H_2O}/N_{O_2} in the centre region (shaded grey in panel e) is shown at the bottom.

constituent is atomic oxygen, O, Molyneux et al. (2018) showed that the required O column densities would put Ganymede's atmosphere in the optically thick range for OI 1 304 Å emission. This would imply that resonant scattering is an important contribution to the OI 1 304 Å intensity. Molyneux et al. (2018) also briefly discuss the morphology in the OI 1 304 Å images from individual exposures, mentioning large regions on the disk where the oxygen ratio is particularly low with $r_{\gamma O} < 1$.

Roth et al. (2021) tested the optical thickness of atomic oxygen atmosphere through a sequence of two exposures with COS before and after Ganymede enters into eclipse, but found no indication that resonant scattering contributes to the OI 1 304 Å emission. The upper limit on the O abundance imposed by this result implies the need for another species causing the measured $r_{\gamma O}$ ratios, which were found to be particularly low on the central trailing hemisphere; see Figure 16.4.

Roth et al. (2021) then showed that the observed oxygen emission ratios are consistent with an H_2O abundance around the central sunlit disks with H_2O/O_2 abundance ratios of 12–32 on the trailing side and 2–5 on the leading side. Around the sub-solar point, dissociative excitation of H_2O contributes significantly to the OI 1 304 Å emission, effectively reducing the oxygen ratio. We note that in all scenarios, the OI 1 356 Å emission almost exclusively originates from electron impact on O_2.

The higher H_2O/O_2 ratio above the warmer trailing hemisphere compared with the colder leading hemisphere and the spatial concentration at the sub-solar region make sublimation the most plausible source for this H_2O atmosphere. In addition, when assuming a column density for O_2 of $\sim 3\times10^{14}$ cm^{-2}, the resulting H_2O column densities are $\sim 10^{15}$ cm^{-2}, also consistent with expected abundances from ice sublimation at Ganymede's maximum surface temperature.

16.2.5 New Horizons P-Alice Observations

The New Horizons (NH) spacecraft observed Ganymede with the Pluto-Alice (P-Alice) instrument during its Jupiter encounter in 2007. The P-Alice UV imaging spectrograph spectrally images extreme- and far-ultraviolet light from 520 Å to 1 870 Å (Stern et al., 2008). P-Alice monitored the OI 1 356 Å and OI 1 304 Å emissions during two eclipse passages of Ganymede (denoted GEclipse01 and GEclipse02) from before ingress through after egress, viewing the sunlit sub-Jupiter (sub-observer W longitude $\sim 9°$, on February 27) and night-side anti-Jupiter (sub-observer W longitude $\sim 155°$, March 4), respectively.

Figure 16.5 shows that the disk-averaged oxygen OI 1 356 Å intensities measured in each event remain relatively stable over the ~200-minute time scale, with possible small increases of some 10 to 20 per cent from pre-ingress through eclipse to past egress. The stability of the OI 1 356 Å emissions, which almost exclusively originates from electron impact on O_2, suggests a stable O_2 atmosphere through the eclipse passage, assuming changes in electron excitation do not counterbalance changes in the atmosphere.

https://doi.org/10.1017/9781108966474.017 Published online by Cambridge University Press

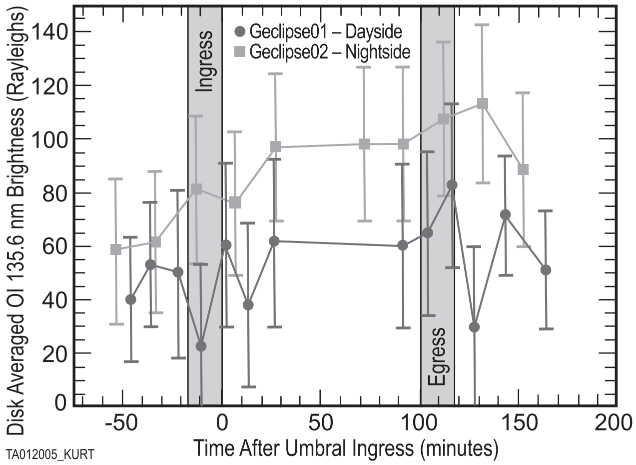

Figure 16.5 New Horizons Pluto-Alice observations of Ganymede's oxygen emissions obtained in 2007 provide the first views of nightside auroral emissions and generally demonstrate a stability of signals during the passage into and out of eclipse for both dayside (GEclipse01) and nightside (GEclipse02) hemispheres.

Moreover, the intensity in the second P-Alice eclipse event (GEclipse02), viewing primarily the nightside hemisphere (one week after the first event – GEclipse01 – that viewed the dayside), suggests that O_2 is similarly abundant on the nightside. The 50 per cent higher intensity of GEclipse02 compared to GEclipse01 might be attributed to the different Jovian magnetospheric plasma conditions at Ganymede. As HST observations are limited to the dayside, the P-Alice GEclipse02 data provide the first evidence for Ganymede's nightside atmosphere.

The analysis of the weaker oxygen OI 1 356 Å is hampered by the interfering surface reflections and possible extended cloud emissions. The average intensity for each event suggests OI 1 356 Å/OI 1 304 Å ratios between 1 and 3 on both days, consistent with previous results. The low signal-to-noise ratio during the second eclipse (GEclipse02) prevents further interpretation of the oxygen ratio with respect to the atmospheric mixing ratio on the nightside.

16.2.6 Other Atmosphere Observations

Already in 1995, Brown (1997) carried out long-slit spectroscopic observations of Ganymede in the search for emissions from sodium (Na) D1 and D2 lines at 5 896 Å and 5 890 Å, respectively. However, no emissions were detected, and an upper limit for the Na column density of 10^8 cm^{-2} was derived, more than an order of magnitude lower than the extended sodium corona discovered earlier at Europa (Brown and Hill, 1996).

Other noteworthy, yet unpublished observations were carried out by the Herschel Space Observatory (Hartogh et al., 2013). Herschel's Heterodyne Instrument for the Far Infrared (HIFI) measured absorption of the background continuum from Ganymede's surface at the 557 GHz water line. Interestingly, HIFI detected this absorption on the leading hemisphere but not on the trailing side, contrary to the results from HST (Roth et al., 2021). In addition, the derived column density for the leading hemisphere from Hartogh et al. (2013) (which we assume to be averaged over the disk of Ganymede) is about an order of magnitude lower than the value estimated based on the HST results for the same hemisphere.

16.3 SOURCES AND SINKS IN GANYMEDE'S ATMOSPHERE

Since the tenuous atmospheres of the icy moons are constantly replenished on timescales near or below their orbital periods, understanding the sources and sinks is key for understanding the abundance and distribution of the neutrals. In the absence of a direct detection of outgassing plumes, Ganymede's atmosphere is assumed to be produced from its icy surface through (i) solar irradiation (i.e., sublimation and photon-stimulated desorption), (ii) Jovian plasma irradiation (i.e., sputtering; this will be discussed later), and (iii) possibly micro-meteorite and dust grain impacts. Whereas this processing resembles that occurring at Europa, the presence of an intrinsic magnetic field on the plasma flow results in interesting spatial differences in the source rates. Therefore, comparisons between the two moons can help separate the relative importance of the sputtering sources. The most important source and sink mechanisms that act on Ganymede – sketched in Figure 16.6 – are described briefly in the following two sections. For a more detailed description of these, as well as the minor source processes, the reader is referred to Chapter 15 of this book.

16.3.1 Sources

As with other objects with thin atmospheres, the solar flux drives H_2O sublimation and thermal desorption of volatiles, namely release of non-condensable molecules trapped in Ganymede's regolith. Sublimation of H_2O is strongly temperature dependent. Ganymede's maximum surface temperature was measured by the Galileo photopolarimeter to reach $\sim$150 K at the sub-solar point (Orton et al., 1996), though the maximum temperature of the water-ice may be significantly lower. At 150 K, the pure H_2O sublimation flux is equal to $\sim 1\times10^{25}$ m^{-2}s^{-1}, whereas at 120 K, the sublimation flux reaches $\sim 4\times10^{14}$ m^{-2}s^{-1} (cf. Figure 15.2 in Chapter 15). The global sputter flux, on the other hand, was computed by the models that will be described shortly to be of the order of 10^{12}–10^{13} m^{-2}s^{-1}. Sublimation thus clearly dominates as a source process at Ganymede's sub-solar point. Away from the sub-solar point sublimation quickly drops off, and at the nightside temperatures of $\sim$80 K the sublimation flux is negligible. Because the sublimation process is relatively well defined and modelling of it comparably simple, models usually do not focus on the implementation of this release process, but rather on the implementation of the more complex sputter release process. It is noteworthy, though, that even though most of the models that will be presented shortly put little emphasis on sublimation modelling, all of them agree on sublimated H_2O being the main exospheric constituent close to the sub-solar point.

The now extensive laboratory and plasma data sets confirm that the Jovian plasma bombardment is an important source of water products. Ganymede is embedded in the Jovian plasma, which consists of electrons, H^+, O^{n+}, and S^{n+}, as

https://doi.org/10.1017/9781108966474.017 Published online by Cambridge University Press

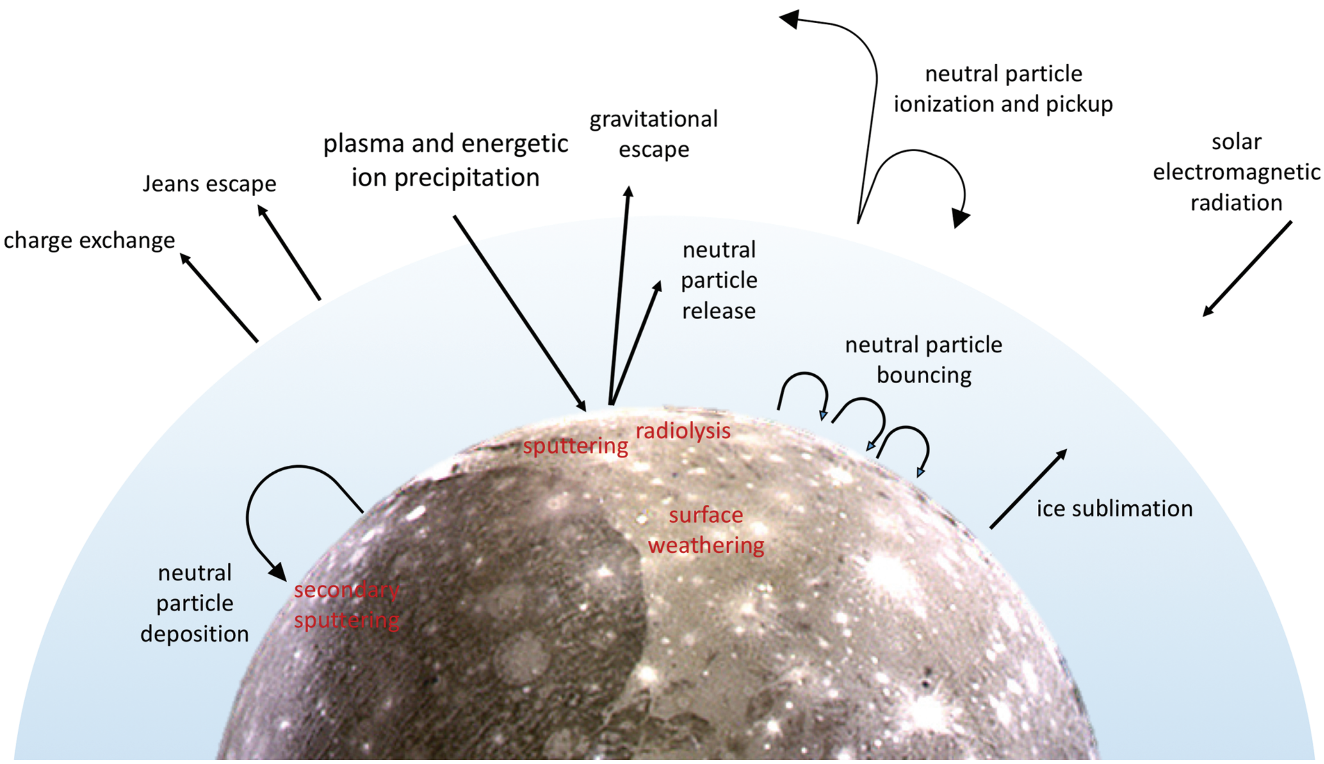

Figure 16.6 Main source and sink mechanisms for Ganymede's exosphere (from Plainaki et al. (2020a)). The moon's environment is strongly coupled with the Jovian magnetosphere through processes that determine the energy exchange between the two systems. Ganymede image credit: NASA/JPL/DLR.

well as trace species with energies of a few eV to MeVs, and moves relative to Ganymede with bulk speeds equivalent to ~160eV/amu (Chapter 3.10). The source of sulphur and oxygen is primarily Iogenic with smaller sources of water products due to atmospheric escape from Europa and Ganymede fueling hydrogen-oxygen neutral tori (Smyth and Marconi, 2006; Marconi, 2007; Smith et al., 2019). Hence, plasma particles reaching Ganymede's surface can produce O_2, O_3, and H_2O_2 in the surface ice grains through a process called radiolysis [Spencer et al., 1995; Noll et al., 1996; Hendrix et al., 1999] and can brighten the polar regions (Johnson, 1997). Plasma bombardment leads to the ejection of H_2O, O_2, H_2, minor water dissociation products, and trace contaminants into the gas phase, a process often referred to as sputtering. Sputtering typically refers to the ejection produced by moment transfer collisions of incident ions with atoms and molecules in the surface of a solid (often referred to as knock-on collisions). Unlike metals [Wood, 1957], which are conductors, ices are weakly bound insulators and therefore can also undergo electronic sputtering, which has been shown to depend on the density of electronic excitations produced in the near-surface region (see figures 2.4 and 3.22b in Johnson (1990)) by impinging ions or electrons (Johnson et al., 2013).

The amount of each species ejected is typically given as a yield, Y, the number of ejected particles per incident particle. These yields depend on the incident plasma particle's energy, impact angle, mass, and charge, and on the temperature of the ice grains. Since the plasma varies temporally and Ganymede's field affects the spatial and energy distributions of particles reaching a surface that is porous and has contaminants, and since the incident plasma implants radicals and causes sintering of the grains, the parameter space of this interaction process is large. Therefore, observational and laboratory data are used synergetically in the modelling efforts.

16.3.2 Sinks

The atmospheric loss rates, as expected, are governed by interaction with solar photons and plasma particles, as well as by escape to space and loss to the regolith. Because of Ganymede's significant gravity, thermal escape is negligible except for the lightest neutrals (H, H_2; Marconi, 2007) or species energized in the gas phase by photon- and plasma-induced dissociation, as well as by charge exchange and momentum transfer collisions with the incident ions, which are also affected by Ganymede's magnetic field (e.g., Leblanc et al. (2017); Carnielli et al. (2020*a*)). Although these sinks exhibit considerable uncertainties, the physical processes are understood. However, the fallback onto the radiation-altered and very porous regolith (85 per cent at the surface: e.g., de Kleer et al. (2021)) and the further fate of the neutrals are not well understood.

Most of the gas phase ejecta return to the surface, where they can condense, react with the grains or permeate the porous regolith as molecules adsorbing and desorbing on the grains (e.g., Oza et al., 2019). The likely important role of the regolith as a potential sink is suggested, for example, by efforts to use the plasma observations to calculate the atmospheric density of O_2 at the icy moons Rhea [Teolis and Waite, 2016] and Ganymede [Leblanc et al., 2017]. Either extremely different models

https://doi.org/10.1017/9781108966474.017 Published online by Cambridge University Press

for the radiolytic production of O_2 are required or the fate of the returning O_2 in their regoliths is very different. Whereas there is considerable laboratory data on the production, much better models for the fate of gas phase species in the icy regoliths are required.

16.4 MODELLING

Much of our understanding of Ganymede's atmosphere is based on modelling efforts, which, very often, incorporate the outputs of extensive laboratory work (e.g., Johnson (1990); Johnson et al. (2004) and references therein). Although the modelling efforts presented in this section are clearly distinct from each other (applying different techniques, focusing on different plasma populations and neutral species, including different interaction processes, analyzing different atmospheric aspects, etc.), they all agree on the general structure of Ganymede's atmosphere: close to the sub-solar point, the atmosphere is dominated by sublimated H_2O molecules, whereas near the terminator and on the nightside the atmosphere is dominated by O_2 close to the surface and by H_2 at higher altitudes.

According to a model implementation by Shematovich (2016), Ganymede's atmospheric environment is characterized by a Knudsen number less than 0.1 up to altitudes of about 50 km, and by a Knudsen number in the range of 0.1–1 at altitudes between $\sim$50 km and a few hundred kilometres. The Knudsen number compares the mean free path of the neutrals between collisions to the local scale of density variations. A Knudsen number (well) below unity indicates a collisional regime. Other modelling efforts (Marconi, 2007; Leblanc et al., 2017) have resulted in similar conclusions, with the atmosphere being collisional or quasi-collisional in a near-surface region near the sub-solar point, and collisionless elsewhere. As a result, some models treat the atmosphere as completely collisionless, while other studies account for neutral–neutral collisions.

Since Ganymede's atmosphere and the Jovian plasma environment are strongly intertwined, it is difficult to investigate one without the other. Atmospheric modelling efforts thus often focus on the Jovian plasma environment and its precipitation onto Ganymede's atmosphere and surface. Yet we remind the reader that sublimation is likely an equally important source but receives less attention solely due to its comparably simple nature.

In the discussion that follows, we first present modelling efforts of the effects of Ganymede's interaction with the magnetosphere on the surface sputtering source as well as the thermal atmosphere source, namely sublimation. Thereafter, we discuss the modelling studies of Ganymede's neutral atmosphere, highlighting new aspects that models included at the time of their introduction.

16.4.1 Modelling of the Sputtering Source

In order to understand where and how surface sputtering releases particles, one first has to understand where and how electrons and ions precipitate onto the moon. This is often accomplished through modelling. Space-based measurements of the environment around Ganymede (e.g., Cooper et al., 2001) have often served as an input for such numerical ion circulation models, which in addition make use of electric and magnetic fields from MHD simulations of Ganymede's environment.

Single-particle Monte Carlo simulations of the circulation and precipitation of energetic ions onto the moon can then indicate the surface regions where intense sputtering and radiolysis are expected (Carnielli et al., 2020*a*; Plainaki et al., 2015; Plainaki et al., 2020a; Plainaki, et al., 2020b). Such ion and electron trajectory computations have been performed for particles in a wide energy range (keV – MeV) for different configurations between Ganymede's magnetic field and Jupiter's plasma sheet: namely the moon above, inside and below the plasma sheet (e.g., Poppe et al. (2018); Plainaki et al. (2020a); Liuzzo et al. (2020); Carnielli et al. (2020*a*)). Such simulations have confirmed the existence of a shielded region close to the trailing hemisphere surface (due to the presence of an internal magnetic field) and enhancements in the ion flux at near-surface altitudes above the low-latitude leading hemisphere. In general, current modelling efforts agree in that ions precipitate predominantly at the moon's polar cap regions along open magnetic field lines, consistent with Ganymede's surface brightness map (Khurana et al., 2007).

As the Jovian plasma consists of electrons and different populations of ions, studies have been undertaken to determine which particles are most relevant for sputtering. According to these modelling efforts, even though the thermal ion precipitation flux of the corotating plasma is similar to the energetic ion precipitation flux (Carnielli et al., 2020*b*), it is the latter that primarily determines the atmosphere sources [Cooper et al., 2001; Gomis et al., 2004; Teolis et al., 2017; Plainaki et al., 2020a] due to the increase in sputter yield with energy in the relevant energy region, and it is also the latter that controls surface weathering (e.g., Johnson (1990); Shi et al. (1995); Khurana et al. (2007)).

Recently, Carnielli et al. (2020a) modelled precipitation of ionospheric ions (in addition to the Jovian plasma ions) onto Ganymede's surface to determine the ionosphere-induced sputter flux and its relative importance. The authors calculated that at least 10 per cent of the overall sputter flux could be due to ionospheric ions, and argued that this contribution could even become the dominant sputtering source under certain assumptions for not-well-constrained parameters such as the O_2 density and ionization frequency. The authors also found that an O_2 column density of $>10^{15}$ cm^{-2} (about 10 times higher than in other studies) is required to match the electron density profiles derived from Galileo measurements.

16.4.2 Modelling of Thermal Sources

Following the identification of energetic ions at Jupiter by Voyager 1 (Krimigis et al., 1977), a *sublimated* water-based atmosphere was suggested to transiently overwhelm the directly sputtered atmosphere predicted at Ganymede by Johnson et al. (1981) based on the equilibrium vapor pressure of H_2O ice. That is, while Europa experiences temperatures approaching $\sim$135 K, equatorial temperatures on Ganymede approach $\sim$150 K near noon, local time. For a collisionless atmosphere (Section 16.4.4) the canonical water column density is a product of the ballistic hop time and a sublimation flux Φ_{sub}, which can be expressed as $\Phi_{sub} = aT^{1/2}exp(-b/T)$, where a and b are empirical parameters constrained by vapor pressure experiments (Table 16.3).

https://doi.org/10.1017/9781108966474.017 Published online by Cambridge University Press

Table 16.2 *Models of Ganymede's neutral atmosphere: *Collisionless and † Collisional. ‡ Sublimation refers to H_2O sublimation in this table. Rates can be found in* Feistel and Wagner (2007) *or* Fray and Schmitt (2009)*. Ch-ex refers to charge exchange. * See also* Plainaki et al. (2020a) **** Carnielli et al. (2019, 2020a,)*.*

Model	**Species**	**Source**	**Loss**	**Novelty**	**Implications**
Johnson et al. (1981)*	O_2, H_2O, H_2, H, OH	Sputtering, Sublimation‡	sticking, e-/photo-dissociation, escape	1st analytic Model	Prediction of O_2 and H_2O atmospheres on icy moons
Marconi (2007)†	O_2, H_2O, H_2, O, H, OH	Sputtering, Sublimation	sticking, e-/photo-dissociation, escape	2-D axisymmetric	Atmospheric profile; Latitudinal distributions: H_2O subsolar; O_2 elsewhere
Turc et al. (2014)*	O_2, H_2O, H_2, O, H, OH	Sputtering, Sublimation	e-/photo-dissociation, escape	3-D Model, Atm. collapse in eclipse	Collisional atm. at noon; H density underestimated
Plainaki et al. (2015)*	O_2, H_2O	Sputtering, Sublimation, Radiolysis	sticking, e- impact dissociation, ch-ex, escape	Plasma precipitation patterns*	Sputtered H_2O variability: leading/trailing; poles/equator; 2-component O_2 atm.
Shematovich (2016) †	O_2, H_2O, H_2, O, H, OH	Sputtering, Sublimation	e-/photo-dissociation, ch-ex	Collisions important	Suprathermal O
Leblanc et al. (2017) †	O_2, H_2O, H_2, O, H, OH	Thermal Radiolysis, Sputtering, Sublimation	sticking, e-/photo-dissociation, escape	3-D Rotational**	H_2O variability: Poles/Noon & leading/trailing; Dusk-over-Dawn O_2 Bulge
Oza et al. (2018)*	O_2	Outgassing, Thermal Radiolysis, Sputtering	e- impact dissociation	1-D Semi-Analytic Atm. Rotation Model	Dusk-over-Dawn O_2 Bulge; presence of near-infinite, outgassing O_2 reservoir
Vorburger et al. (2022)*	H_2O	Sputtering, Sublimation	sticking, e-/photo-dissociation, e-/photo-ionization, escape	Ion- and electron-sputtering, plasma precipitation patterns	Sublimation-dominated regions constrained, importance of $O^{+,++}$ and S^{+++} sputtering, electron-sputtering negligible

Along with the direct phase transition into sublimated water vapor, the desorption of the radiolytic O_2 that permeates the regolith (Oza et al., 2018; Johnson et al., 2019) and potential H_2O outgassing (Roth et al., 2014) as at Europa might also occur at Ganymede. Nevertheless, at present, observational evidence of a H_2O column at Ganymede remains to be confirmed against these predictions, presenting an avenue for characterization for future observers. In the following section we discuss simulations in an effort to characterize the preceding sources and sinks based on various assumptions, for example, collisional (Section 16.4.3), collisionless (Section 16.4.4), and rotation (Section 16.4.5).

16.4.3 Collisional and Quasi-Collisional Atmosphere Models

The 2-D axisymmetric kinetic model by Marconi (2007) used a multispecies approach to derive the atmospheric H_2O, O_2, H_2, O, H, and OH spatial structures. The model included implementation of a non-uniform surface temperature distribution, energetic plasma energy spectra as measured by the Galileo energetic particle detector when Galileo was near Ganymede, and energy-dependent sputter yields, which are based on laboratory studies. The authors found that near the sub-solar point the dominant component is sublimated H_2O vapor, whereas near the polar regions the main component is molecular oxygen

https://doi.org/10.1017/9781108966474.017 Published online by Cambridge University Press

Table 16.3 *Pure H_2O ice grain sublimation flux parameters for a simplistic sublimation model.* Adapted from Oza (2017) Figure 3.5, *p. 93. We note that all experimental measurements to our knowledge of H_2O, summarized in Fray and Schmitt (2009), range from 130 to 273.15 K encouraging the need for more experiments at low temperatures.*

Model	a	b
	[cm^{-2} s^{-1}]	[K]
Johnson et al. (1981)	1.9×10^{32}	6 146
Marconi (2007)	1.1×10^{30}	5 737
Fray and Schmitt (2009)†	2.2×10^{32}	5 950
Leblanc et al. (2017)	1.9×10^{32}	8 500

† Fray and Schmitt (2009) use a more complicated formula for the sublimation flux, which we have interpolated to the simpler form for this comparison.

at low altitudes and molecular hydrogen at high altitudes, two species that do not condense easily and thus accumulate in the atmosphere (see Figure 16.7). A similar approach was also followed by Shematovich (2016) who used a kinetic model to investigate the near-surface atmosphere, taking collisions into account, and the extended atmosphere by including atmospheric sputtering and thermalization of supra-thermal atoms. The authors found that collisions caused the 10–100 km altitude to be populated by both O_2 and H_2O, and that inclusion of atmospheric sputtering and thermalization of supra-thermal atoms resulted in a substantial increase in the scale height of these species. These results were later confirmed by Leblanc et al. (2017) who used a 3D multi-species collisional approach (see the following discussion).

16.4.4 Collisionless Exosphere-Type Models

Several models have used a Monte-Carlo model approach to treat Ganymede's neutral gas environment as an exosphere, that is, neglecting collisions between atmospheric particles. Turc et al. (2014) applied a collisionless 3D model approach for simulating Ganymede's exosphere above the sunlit trailing hemisphere. The obtained exosphere confirmed the results that were obtained by the kinetic model of Marconi (2007), namely that sputtering and sublimation result in a strong dichotomy between the sub-solar region, where H_2O sublimation dominates, and the rest of the surface, where O_2 and H_2 dominate. In addition, the authors studied Ganymede's atmospheric response to time-varying parameters, namely Ganymede passing into the shadow of Jupiter and intrinsic variations in the Jovian plasma (for the results of these analyses see Section 16.4.5).

The exospheric model by Plainaki et al. (2015) was the first to account for the intensity and spatial distributions of the precipitating Jovian ions onto Ganymede's surface and to derive the induced surface-sputtered flux. They showed that sputtering alone would produce an H_2O distribution confined to mostly the polar regions and the low-latitude wake hemisphere, whereas sublimation releases H_2O in the sub-solar region; see Figure 16.8. The modelled O_2 exosphere comprises a nearly globally uniform and relatively dense part, one that is close to the surface and consists mainly of thermal molecules (molecules thermalized to surface temperature), and a less homogeneous part consisting of more energetic O_2 molecules resulting from direct surface sputtering, with a spatial distribution that depends on both the plasma surface impact and surface temperature. In addition, Plainaki et al. (2020a) investigated ion precipitation onto Ganymede's surface for different relative configurations between the moon's magnetic field and Jupiter's plasma sheet, that is, when Ganymede is above, close to the centre of, and below the Jovian plasma sheet, and found that the sputtered H_2O flux can easily change by an order of magnitude.

Finally, like Plainaki et al. (2015), Vorburger et al. (2022) accounted for the intensity and spatial distributions of the precipitating magnetospheric H^+, O^+, O^{++}, and S^{+++} ions onto Ganymede's surface, but also included electron precipitation fluxes in their analysis. The authors confirmed the H_2O distribution found earlier by Marconi (2007), Turc et al. (2014), and Plainaki et al. (2015), and showed that sputtering of the water atmosphere is mainly induced by the heavy ions, while protons and electrons play only a very minor role. In addition, their modelled H_2O atmosphere is in good agreement with the observations of a sublimated water component (Roth et al., 2021).

16.4.5 Atmosphere Models Including Orbital Variability

Leblanc et al. (2017) advanced the 3D model of Turc et al. (2014) in order to describe the orbital evolution of the atmosphere, by taking into account Jupiter's gravitational influence, the plasma upstream (trailing)/plasma wake (leading) orbital asymmetry, and Ganymede's rotation. They find that Ganymede's sublimated and sputtered atmosphere has a characteristic timescale (τ_i), determined primarily by electron-impact dissociation and ballistic flight times, which is similar to Ganymede's rotational period (τ_{orb}). This implies that Ganymede's atmosphere at a given orbital position is strongly dependent on the atmospheric source and sink processes occurring earlier in the orbit. In other words, in the absence of sources, the atmosphere is destroyed in less than one Ganymede day and is shaped by what happened earlier in the day. Figure 16.9 illustrates the consequences of the orbital evolution, most pronounced in O_2.

Such rotation-driven asymmetries are most apparent in the abundance of comparably long-lived volatiles like O_2. On Earth's Moon, non-condensable volatiles such as Ar exhibit a similar dusk-over-dawn asymmetry due to the balance of sources and sinks over an orbit. Hodges and Johnson [1968] tracked the latitudinal evolution of volatiles via density gradients. Recently Oza et al. (2018) used a simple analytic model to track the longitudinal evolution of the column density of a volatile. In this way, they examined the effect of atmospheric source properties on the longitudinal distribution of O_2

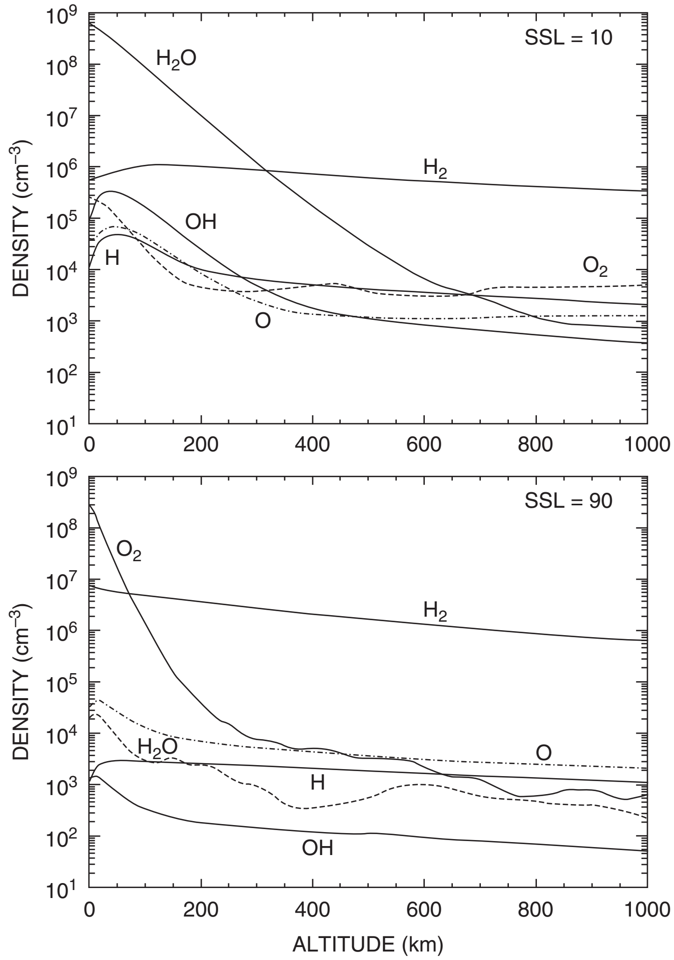

Figure 16.7 Atmospheric density profile at a sub-solar latitude (SSL) of 10° (a) and 90° (b), from Marconi (2007), suggesting a two-part atmosphere with a dominant sublimated H_2O atmosphere near the sub-solar point (upper panel) and a primary sputtering O_2 atmosphere elsewhere. This was later confirmed and supported by various models and observations. Reprinted from *Icarus*, 190(1), M.L. Marconi, A kinetic model of Ganymede's atmosphere, 155–174., ©2007, with permission from Elsevier.

in a surface-bounded atmosphere on tidally locked satellites, including Ganymede.

By modelling the atmospheric source and sink (Section 16.3) processes to assess the longitudinal and, therefore, time *evolution* of the atmospheric column density N in the form

$$\left(\frac{dN}{dt}\right) = Source - (Sink) \times N, \tag{16.1}$$

the atmospheric evolution parameter $\beta = 2\pi \frac{\tau_i}{\tau_{orb}}$, the ratio of the atmospheric lifetime to the diurnal timescale of the satellite, was shown to be critical. When β is very large, there is little longitudinal dependence, and when very small, the column is dominated by production. As β approaches unity, a dusk-over-dawn asymmetry can appear, similar to a thermal tide. This has been shown to account for the observed dusk/dawn enhancement in O_2 at Europa (Roth et al., 2016). That is, the radiolytically produced but returning O_2 permeates its porous regolith, providing a *thermal* source of O_2 that is much less sensitive to the local radiolytic production rate from the surface ice. A peak abundance near dusk local time is similarly expected for Ganymede (Leblanc et al., 2017; Oza et al., 2018) based on the estimated atmospheric residence time of O_2, which is similar to Ganymede's orbital period. In this picture, radiolysis-induced desorption of O_2 from its icy regolith is an important source at Ganymede as well as Europa (Johnson et al., 2019). Leblanc et al. (2017) also suggested that, even if the atmospheric O_2 molecules are preferentially ejected from the polar regions by sputtering, they will tend to accumulate in the regolith in the equatorial region as their many ballistic hops are affected by the centrifugal acceleration.

Several models (Plainaki et al., 2015; Leblanc et al., 2017) have suggested trailing-over-leading asymmetries of H_2O. Since H_2O freezes upon surface contact, it has a much shorter lifetime compared to O_2 and the distribution of H_2O is closely related to its source regions. Since Ganymede's trailing hemisphere has a lower albedo than the leading hemisphere (Spencer et al., 1989), the trailing hemisphere surface temperature is expected to be higher (Leblanc et al., 2017). Assuming the same level of contamination of the ice everywhere, highest sublimation flux is expected near the sub-solar point when the trailing hemisphere is illuminated, while the sublimation H_2O atmosphere is less dense on the sunlit leading hemisphere. The maximum sputtering flux, in contrast, is expected near the poles (Plainaki et al.,

https://doi.org/10.1017/9781108966474.017 Published online by Cambridge University Press

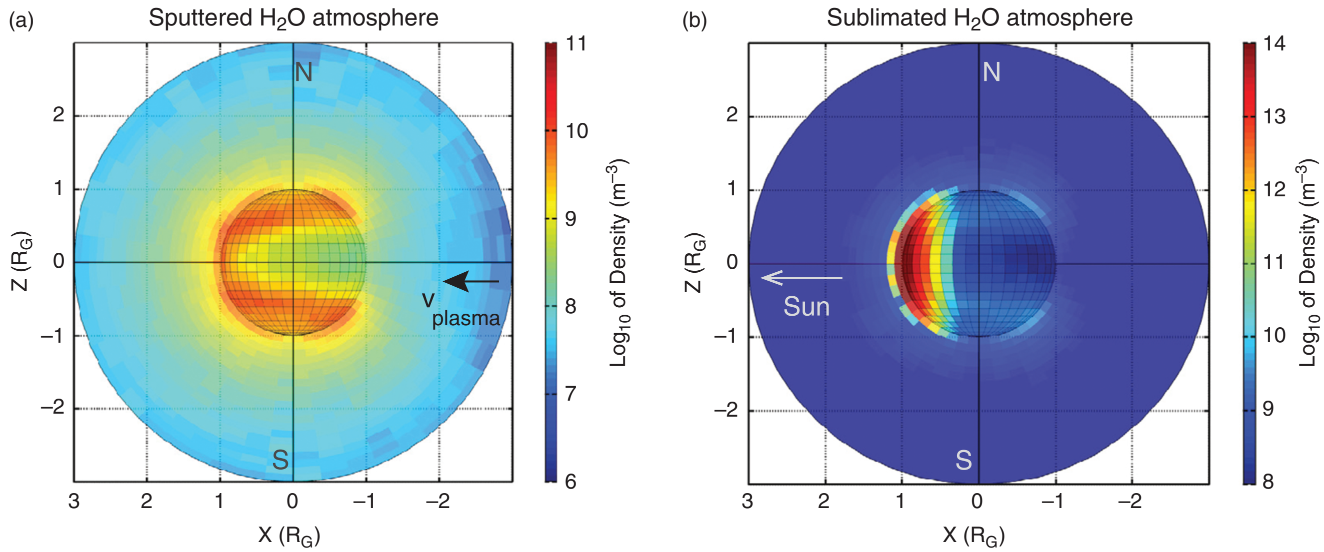

Figure 16.8 Projected atmospheric H_2O density distributions over the surface of Ganymede and in a plane through Ganymede's centre, where X is along the ambient plasma flow direction (shown by the black arrow) and Z is along Jupiter's spin axis (in units of Ganymede's radii, North 'N' is up), adapted from Plainaki et al. (2015). The Sun is to left, shown by the grey arrow. Panel a shows the H_2O that is produced from surface sputtering only, where H_2O is mostly confined to the regions near the open field lines. Panel b shows H_2O from sublimation only, with H_2O confined to the dayside. The peak sublimated density near the sub-solar points exceeds the maximum sputtered density by three orders of magnitude (note the different ranges of the color bars). Reprinted from *Icarus*, 245, Christina Plainaki, Anna Milillo, Stefano Massetti, Alessandro Mura, Xianzhe Jia, Stefano Orsini, Valeria Mangano, Elisabetta De Angelis, Rosanna Rispoli, The H_2O and O_2 exospheres of Ganymede: The result of a complex interaction between the jovian magnetospheric ions and the icy moon, 306–319, ©2015, with permission from Elsevier.

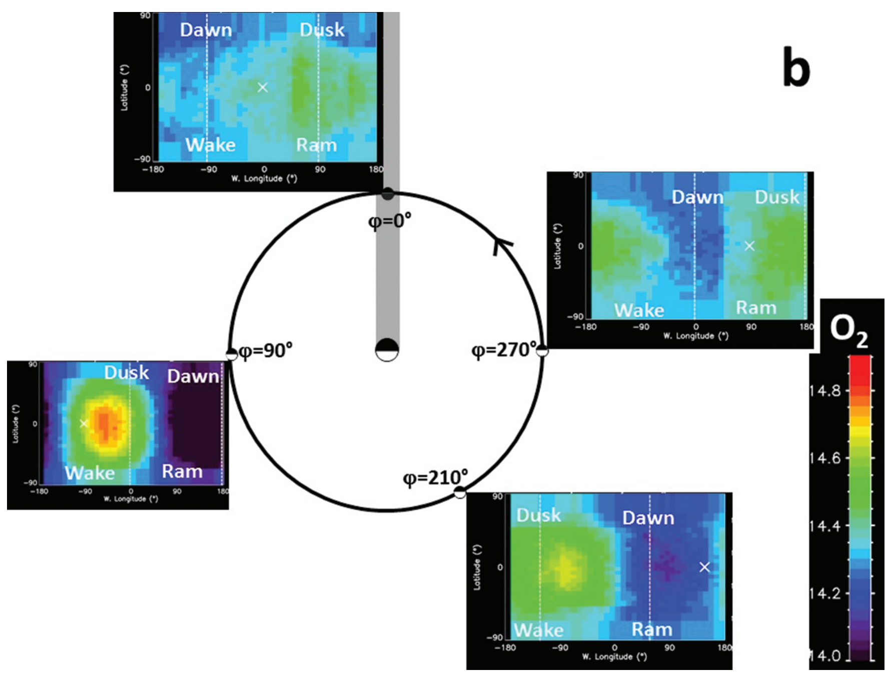

Figure 16.9 Simulated atmospheric evolution maps (latitude vs. W longitude) of zenith O_2 column densities at four Ganymede phase angles, from Leblanc et al. (2017). To follow diurnal behavior, the sub-solar point is indicated by an 'X' and dusk/dawn terminators are represented by the vertical dashed white lines. To follow plasma behavior, ram and wake are labeled. Ganymede's angular rotation vector Ω is counter-clockwise in the plane of Jovian co-rotation. Reprinted from *Icarus*, 293, F. Leblanc, A. V. Oza, L. Leclercq, C. Schmidt, T. Cassidy, R. Modolo, J. Y. Chaufray, R. E. Johnson, On the orbital variability of Ganymede's atmosphere, 185–198, ©2017, with permission from Elsevier.

Table 16.4 *Surface density and column density ranges derived from atmospheric models. Values in parentheses are derived from observations, stated here for comparison.*

Species	Density [cm^{-3}]	Column Density [cm^{-2}]	Resident time [s] – limiting loss process†	References
H_2O (sub-solar)	2e8–4e9 (2e8–1e9)	6e15–2e16	3e2–1e3 – return to surface	*a,b,c,d,e,f*
H_2O (polar)	4e3–3e4	2e11–3e11		*a,b,c,d,f*
O_2	1e7–9e7 (1e8)	4e13–2e15 (3e13-1e15)	1e3–7e5 – dissociation/ionization	*b,c,d,e*
H_2	1e5–8e6	1e14–1e15	4e4–1e5 – escape	*a,b,d,e*
OH	∼(1e2–1e4)	∼(1e10–1e12)	∼(1e3–1e5) – escape/return to surface	*a,b,d*
O	∼1e4	∼1e12	∼1e4 – escape/return to surface	*a,b,d*
H	∼5e3	∼1e12	∼1e4 – escape	*a,b,d,e*

†Resident time in the atmosphere and the relevant limiting process that determines the time scale, [a]Marconi (2007), [b]Turc et al. (2014),[c]Plainaki et al. (2015), [d]Shematovich (2016), [e]Leblanc et al. (2017), [f]Vorburger et al. (2022).

2015; Leblanc et al., 2017; Vorburger et al., 2022) (Figure 16.8). Depending mostly on the H_2O lifetime and surface thermal inertia, the dayside sublimation H_2O atmosphere should collapse or fade during an eclipse passage of Ganymede (Leblanc et al., 2017).

16.5 SUMMARY AND PERSPECTIVES

16.5.1 Summary of Observational and Modelling Work

Since the first detections in the mid-1990s and with the following increased model effort, substantial progress has been made in characterizing and understanding Ganymede's tenuous atmosphere.

On the observational side, the disk-integrated intensities of the OI 1 304 Å and OI 1 356 Å oxygen emissions from the atmosphere suggest that the majority of the total signal originates from dissociative excitation of molecular oxygen, O_2. At higher altitudes, namely in the extended exosphere, the observations are consistent with an increased mixing ratio of atomic oxygen to molecular oxygen.

However, interpreting the observations of the electron-excited oxygen emissions is generally limited by the fact that the signal is affected by the properties of both the neutral gas and the electrons as exciting species. Given the lack of knowledge about the distribution and temperature of the electrons (i.e., their phase space density), it is impossible to extract reliable constraints on absolute abundances or spatial distributions of individual molecules or atoms. Hence, the available data does not allow one to test hypotheses about asymmetries, inhomogeneities, or temporal variability in the atmospheric abundances.

The relative intensity of the OI 1 304 Å and OI 1 356 Å emissions is a diagnostic for mixing ratio. As such, it is less sensitive to the electron properties compared to the absolute intensities as a diagnostic for absolute abundance.

With a global OI 1 356 Å/OI 1 304 Å ratio that has been found to be around 2 (roughly between 1.3 and 2.7), electron excitation of O_2 is the overall primary emission source. The nightside observations by New Horizons as well as observations when Ganymede is eclipsed by Jupiter confirmed the presence of stronger OI 1 356 Å than OI 1 304 Å even in absence of solar illumination. However, it was found that the oxygen ratio systematically decreases from the limb region towards the central disk region, which coincides with the sub-solar region in HST images. The systematically changing ratio is consistent with an atmosphere that transitions from being O_2 dominated near the terminator (and on the nightside) to an H_2O-dominated atmosphere on the central dayside.

Simulation efforts generally produce results that are well in agreement with these observational constraints, providing additional context to improve the understanding. Table 16.4 gives rough ranges of the surface densities, column densities, as well as atmospheric resident times for all modelled water group species, derived and estimated from various models. We note that this is a simplification and some results might not be considered if they differ significantly from the usual ranges. The given numbers are mostly in agreement with the few observational constraints at hand. The simulations predict a number of characteristics, which remain to be confirmed by future missions and observational campaigns.

Given the various sources (sublimation, ion and electron sputtering, desorption) and their specific characteristics, all models predict an inhomogeneous and temporally variable (mostly on the timescale of Ganymede's orbit) atmosphere. Differences in the abundance and distribution of O_2 over an orbit are expected due to the changing geometry and in particular the change in the plasma stream direction and thus the related topology of Ganymede's mini-magnetosphere relative to the solar illumination. The presence and even dominance at higher altitudes of molecular hydrogen, H_2, is also consistently predicted. For the nightside, the simulations suggest an O_2-dominated atmosphere, since the sputtering and radiolysis source for O_2 has a comparably small dependence on surface temperature (and thus time of day) and the long lifetime of the O_2 molecules is similar to the orbital period. Molecular hydrogen is similarly expected to be globally abundant.

Various properties remain overall unclear. One example is the uncertainty of the surface ice properties (temperature, contamination level, porosity, reactions in the regolith) and of the resulting sublimation yield. Furthermore, until advanced spacecraft measurements rule this out, it remains a possibility that localized sources such as outgassing plumes like those on Enceladus (Hansen et al., 2020) and possibly Europa (Roth et al., 2014) are present on Ganymede.

16.5.2 Brief Comparison to Europa and Callisto

Ganymede's atmosphere can be expected to have many similarities to the atmospheres of Europa and Callisto. The main sources are likely charged particle sputtering and sublimation, as all three are embedded in Jupiter's (nearly) co-rotating magnetospheric plasma and their outermost layers consist predominantly of water-ice.

However, there are also differences in the properties of both the moons themselves and their environments. The magnetospheric plasma density and strength of Jupiter's magnetic field decreases from Europa out to Callisto by roughly two orders of magnitude, leading to differing plasma interactions (Kivelson et al., 2004) and particle sputtering efficiency and distribution. In addition, Ganymede has the internal magnetic field that affects the regions where charged particles can impinge onto the surface as discussed in detail previously. The difference in plasma environment also affects the atmospheric losses related to plasma collisions.

On the other hand, the characteristics of the icy surfaces also differ (Greeley et al., 2004; Pappalardo et al., 2004; Moore et al., 2004). Europa's surface is youngest with the highest ice content, and the moon's albedo is highest and surface temperatures thus the lowest. Callisto's surface is oldest and most contaminated, making it overall darker and likely warmer. Ganymede is again in between in terms of the surface properties like contamination, albedo, and temperature. These differences can lead to significantly different sublimation yields and also affect the sputtering yields of the water group species (Spencer, 1987).

The atmospheres of all three moons have been observed through the FUV oxygen emissions, confirming some of the expected similarities and differences. In all cases, the strongest contribution to the oxygen emissions is interpreted to originate from electron-impact dissociated excitation of O_2 (Hall et al., 1998; Cunningham et al., 2015). The properties of the exciting electrons are yet different: at Europa, the thermal plasma electrons are thought to excite the emissions (Roth et al., 2016). At Ganymede, the particular band shape of the emissions and the strong local intensities hint at electrons that are locally accelerated. Callisto's emissions are most consistent with airglow, meaning that low-energy photo-electrons excite the neutrals, while the magnetospheric electrons are effectively diverted around the moon (Strobel et al., 2002). The FUV signal near the disk centre that was related to a sublimated H_2O atmosphere at Ganymede (Roth et al., 2021) was similarly found at Europa but only on the darker trailing hemisphere (Roth, 2021). This is consistent with the expectation that sublimation is overall less effective at Europa than at Ganymede due to the lower surface temperature. The faint airglow signals from Callisto's atmosphere have not (yet) provided means to properly constrain the abundance of species other than O_2. The infrared detection of CO_2 in Callisto's atmosphere (Carlson, 1999) was possible due to a fortunate observing geometry during a flyby of the Galileo spacecraft. Carbon dioxide might be present in the atmospheres of Europa and Ganymede as well.

16.5.3 Future Observations

After more than 30 years in space, the Hubble Space Telescope is still operating and there are two new programs for FUV observations of Ganymede being carried out in 2021. In addition, the NASA Juno spacecraft performs two flybys at Ganymede the same year, with the possibility to provide new insights on Ganymede's atmosphere from its in situ and remote-sensing instruments. The long-awaited James Webb Space Telescope (JWST) was launched on 25 December 2021. The JWST has the potential to map different species in the atmosphere such as H_2O and CO_2 at infrared wavelengths. Ganymede is one of several targets in a granted JWST Early Release Science program, which aims at learning and testing JWST's capabilities to probe the Jupiter system.

Hence, hopes are high that we get more observational constraints on Ganymede's atmosphere in coming years. A large step forward is expected through the JUICE mission scheduled to arrive at Jupiter around 2030.

16.5.4 JUICE Investigation Plans

A major science objective of the JUICE mission is the characterization of Ganymede as a planetary object and possible habitat (Grasset et al., 2013), including a detailed investigation of Ganymede's tenuous atmosphere and its interaction with the Jovian magnetosphere. Both in situ and remote-sensing instruments will contribute measurements to constrain atmospheric composition, structure, temperature, and volatile content, and repeated observations over multiple flybys and throughout the Ganymede orbit mission phase will facilitate studies of atmospheric variability. In situ measurements by the Particle Environment Package (PEP) instrument suite will be used to determine the neutral composition at low altitudes, while remote-sensing instruments will map emission and absorption features of key atmospheric species in the ultraviolet, visible-NIR, and submm spectral regions, respectively. Spectral images of reflected sunlight obtained will also allow surface composition and variability to be investigated, providing valuable information about atmospheric sources and sinks.

The JUICE UltraViolet imaging Spectrograph (UVS) will map neutral emissions of hydrogen (1 216 Å) and oxygen (1 304 Å and 1 356 Å) at spatial resolutions on the order of a few kilometers, allowing the distribution and column density of O, O_2, and H_2O in Ganymede's atmosphere to be derived. Limb stares will be used to investigate the vertical structure of the atmosphere and will also provide opportunities to search for fainter signatures of potential minor atmospheric species such as S, C, and Cl, which have prominent emissions in the 1 000–2 000 Å wavelength region. UVS will also measure O_2 and H_2O in absorption by observing the attenuation of stellar (or solar) light as the star (Sun) is occulted by Ganymede's atmosphere. Occultation spectra will also be assessed for the presence of additional minor species with distinctive absorption features in the 510–2 040 Å UVS bandpass, including CO_2, SO_2, and O_3. Complementary observations of the UV surface reflectance will help to constrain the sources and sinks of the atmosphere, since key volatile species including H_2O, CO_2, and SO_2 have characteristic reflectance features in the far ultraviolet (e.g. Hapke et al., 1981).

https://doi.org/10.1017/9781108966474.017 Published online by Cambridge University Press

The Moons And Jupiter Imaging Spectrometer (MAJIS) is a compact visible and near-infrared imaging spectrometer covering the spectral range from 0.5 to 5.54 μm (Guerri et al., 2018; Langevin et al., 2018; Piccioni et al., 2019). The MAJIS system has the potential to observe the non-LTE photon emission from Ganymede's water vapor exosphere in the 2.4–3 μm range through limb measurements. A first preliminary evaluation of such a potential was performed by Plainaki, et al. (2020b), considering two representative observation cases with the instrument orbiting at an altitude of 5 000 km above the moon's surface: one at high vertical resolution (projected instantaneous field of view of ∼1.1 km) and one at low vertical resolution (projected instantaneous field of view of ∼10 km). The estimations showed that the instrument's sensitivity to the moon's water vapor environment reaches a SNR of 1 during limb observations with tangent at an altitude of 100 km at low latitudes (with higher SNR for lower altitudes). Although ion sputtering contributes in the release of water molecules in Ganymede's environment, the dominant exosphere generation mechanism is sublimation (Marconi, 2007; Plainaki et al., 2015; Shematovich, 2016). As a result, for the aforementioned geometry, the expected MAJIS sensitivity will allow one to measure Ganymede's sublimated-water exosphere.

The Submillimetre Wave Instrument (SWI) is a heterodyne spectrometer, consisting of two channels that measure spectra in wavelength ranges around 520 μm (530 GHz–625 GHz) and 250 μm (1080–1275 GHz). The SWI spectrometer will map the emission and absorption of the water isotopes $H_2^{16}O$, $H_2^{17}O$, $H_2^{18}O$, HDO, and the ortho-to-para ratio of gaseous water (a proxy for the conditions under which the water formed) as well as the CO molecule. Additionally, SWI can be tuned to 80 other molecules that partly may be present in plumes, characterizing evolutionary processes of the interior of the Galilean moons. Due to the high spectral resolution of SWI (>107), the exact position and shape of the molecular lines can be determined. This allows one to not only derive number densities of the molecules but other physical parameters like the transition region between collision- and non–collision-dominated regions in the moons' atmospheres as well as wind and temperature profiles. The capabilities of heterodyne spectrometers like SWI have been demonstrated for LTE and non-LTE conditions in one to three dimensions on comets (Hartogh et al., 2010, 2011b; Rezac et al., 2019), and the Enceladus torus (Hartogh et al., 2011a) and simulations for Ganymede have been recently published (Yamada et al., 2018; Wirström et al., 2020).

The Neutral and Ion Mass (NIM) spectrometer of the PEP instrument suite is a compact, high-resolution, time-of-flight mass spectrometer designed to measure thermal (<5 eV) atmospheric neutrals and ions in the mass range 1–1 000 u/q, with a mass resolution (M/ΔM) of 1 100 and a detection threshold of 1 cm^{-3} ($\sim 10^{-16}$ mbar) [Föhn et al. 2021]. The NIM spectrometer's design results in a very high dynamic range, covering more than six decades in a single setup and about 12 decades using different gains and integration times. In addition, NIM can take measurements at a high cadence, with one complete mass spectrum becoming available every 5 s at closest approach. The NIM spectrometer will perform the first direct sampling (in situ measurements) of Ganymede's neutral gas environment, determining atmospheric properties with a high degree of confidence, because direct sampling (in contrast to remote sensing) is not affected by the physical properties of the material to be analyzed. It is foreseen that NIM may measure Ganymede's sputtered and sublimated bound atmosphere and possible extended neutral clouds whenever JUICE is closer to Ganymede's surface than 100 000 km, and continuously during the Ganymede orbits. At near-surface altitudes, NIM may be able to characterize atmospheric O_2 bulges, which might occur at certain local times or longitudes (Leblanc et al., 2017; Oza et al., 2018). In addition, NIM's atmospheric measurements will allow determination of the chemical and isotopic composition, density, temperature, and scale height of the neutral atmosphere. The NIM spectrometer will be able to resolve important possible trace species such as Mg, Al, Si, Ca, and Na, and allow identification of isotopes for various elements, depending on their abundance.

Set into the larger context, the JUICE measurements will improve the understanding of the atmosphere of the largest planetary and only known 'magnetic' moon. It will thereby allow more general and systematic comparisons to atmospheres of other bodies in the solar system and beyond.

REFERENCES

Alday, J., Roth, L., Ivchenko, N. et al. (2017), 'New constraints on Ganymede's hydrogen corona: analysis of Lyman-α emissions observed by HST/STIS between 1998 and 2014', *Planet. Space Sci.* **148**, 35–44.

Bagenal, F. and Dols, V. (2020), 'The space environment of Io and Europa', *J. Geophys. Res.* **125**(5), e27485.

Bagenal, F., Sidrow, E., Wilson, R. J. et al. (2015), 'Plasma conditions at Europa's orbit', *Icarus* **261**, 1–13.

Barth, C. A., Hord, C. W., Stewart, A. I. F. et al. (1997), 'Galileo ultraviolet spectrometer observations of atomic hydrogen in the atmosphere at Ganymede', *Geophys. Res. Lett.* **24**(17), 2147–50.

Broadfoot, A. L., Sandel, B. R., Shemansky, D. E. et al. (1981), 'Overview of the Voyager ultraviolet spectrometry results through Jupiter encounter', *J. Geophys. Res.* **86**(A10), 8259–84.

Brown, M. E. (1997), 'NOTE: a search for a sodium atmosphere around Ganymede', *Icarus* **126**(1), 236–8.

Brown, M. E. and Hill, R. E. (1996), 'Discovery of an extended sodium atmosphere around Europa', *Nature* **380**(6571), 229–31.

Brown, W. L., Lanzerotti, L. J. and Johnson, R. E. (1982), 'Fast ion bombardment of ices and its astrophysical implications', *Science* **218**(4572), 525–31.

Brown, W. L., Lanzerotti, L. J., Poate, J. M. and Augustyniak, W. M. (1978), 'Sputtering of ice by MeV ions', *Phys. Rev. Lett.* **49**(15), 1027–30.

Carlson, R. W. (1999), 'A tenuous carbon dioxide atmosphere on Jupiter's moon Callisto', *Science* **283**(5400), 820–1.

Carlson, R. W., Bhattacharyya, J. C., Smith, B. A. et al. (1973), 'An atmosphere on Ganymede from its occultation of SAO 186800 on 7 June 1972', *Science* **182**(4107), 53–5.

Carnielli, G., Galand, M., Leblanc, F. et al. and Jia, X. (2019), 'First 3D test particle model of Ganymede's ionosphere', *Icarus* **330**, 42–59.

Carnielli, G., Galand, M., Leblanc, F. et al. (2020*a*), 'Constraining Ganymede's neutral and plasma environments through simulations of its ionosphere and Galileo observations', *Icarus* **343**, 113691.

Carnielli, G., Galand, M., Leblanc, F. et al. (2020*b*), 'Simulations of ion sputtering at Ganymede', *Icarus* **351**, 113918.

Cooper, J. F., Johnson, R. E., Mauk, B. H., Garrett, H. B. and Gehrels, N. (2001), 'Energetic ion and electron irradiation of the icy Galilean satellites', *Icarus* **149**(1), 133–59.

Cunningham, N. J., Spencer, J. R., Feldman, P. D. et al. (2015), 'Detection of Callisto's oxygen atmosphere with the Hubble Space Telescope', *Icarus* **254**, 178–89.

de Kleer, K., Butler, B., de Pater, I. et al. (2021), 'Ganymede's surface properties from millimeter and infrared thermal emission', *Planet. Sci.* **2**(1), 5–24.

Eviatar, A., Strobel, D. F., Wolven, B. C. et al. (2001), 'Excitation of the Ganymede ultraviolet aurora', *Astrophys. J.* **555**, 1013–19.

Eviatar, A., Vasyliūnas, V. M. and Gurnett, D. A. (2001), 'The ionosphere of Ganymede', *Planet. Space Sci.* **49**(3–4), 327–36.

Feistel, R. and Wagner, W. (2007), 'Sublimation pressure and sublimation enthalpy of H_2O ice Ih between 0 and 273.16 K', *Geochim. Cosmochim. Acta* **71**(1), 36–45.

Feldman, P. D., McGrath, M. A., Strobel, D. F. et al. (2000), 'HST/STIS ultraviolet imaging of polar aurora on Ganymede', *Astrophys. J.* **535**, 1085–90.

Fray, N. and Schmitt, B. (2009), 'Sublimation of ices of astrophysical interest: a bibliographic review', *Planet. Space Sci.* **57**(14–15), 2053–80.

Gomis, O., Satorre, M. A., Strazzulla, G. and Leto, G. (2004), 'Hydrogen peroxide formation by ion implantation in water ice and its relevance to the Galilean satellites', *Planet. Space Sci.* **52**(5–6), 371–8.

Grasset, O., Dougherty, M. K., Coustenis, A. et al. (2013), 'JUpiter ICy moons Explorer (JUICE): an ESA mission to orbit Ganymede and to characterise the Jupiter system', *Planet. Space Sci.* **78**, 1–21.

Greeley, R., Chyba, C. F., Head, I. J. W. et al. (2004), 'Geology of Europa', in Bagenal, F., Dowling, T. E., and McKinnon, W. B., eds., *Jupiter: The Planet, Satellites and Magnetosphere*, Cambridge University Press, pp. 329–62.

Guerri, I., Fabbri, A., Tommasi, L. et al. (2018), The optical design of the MAJIS instrument on board of the JUICE mission, in Mazuray, L., Wartmann, R. and Wood, A. P., eds., *Optical Design and Engineering VII*, Vol. 10690 of Society of Photo-Optical Instrumentation Engineers (SPIE) Conference Series. https://ui.adsabs.harvard.edu/abs/2018SPIE10690E..1LG.

Hall, D. T., Feldman, P. D., McGrath, M. A. and Strobel, D. F. (1998), 'The far-ultraviolet oxygen airglow of Europa and Ganymede', *Astrophys. J.* **499**(5), 475–81.

Hall, D. T., Strobel, D. F., Feldman, P. D., McGrath, M. A. and Weaver, H. A. (1995), 'Detection of an oxygen atmosphere on Jupiter's moon Europa', *Nature* **373**(6516), 677–9.

Hansen, C. J., Esposito, L. W., Colwell, J. E. et al. (2020), 'The composition and structure of Enceladus' plume from the complete set of Cassini UVIS occultation observations', *Icarus* **344**, 113461.

Hapke, B., Wells, E., Wagner, J. and Partlow, W. (1981), 'Far-UV, visible, and near-IR reflectance spectra of frosts of H_2O, CO_2, NH_3 and SO_2', *Icarus* **47**(3), 361–7.

Hartogh, P., Bockelée-Morvan, D., Rezac, L. et al. (2013), Detection and characterization of Ganymede's and Callisto's water atmospheres, in 'Presented at the International Symposium "The Universe Explored by Herschel" 15–18 October 2013, ESTEC, Netherlands'.

Hartogh, P., Crovisier, J., de Val-Borro, M. et al. (2010), 'HIFI observations of water in the atmosphere of comet C/2008 Q3 (Garradd)', *A&A* **518**, L150.

Hartogh, P., Lellouch, E., Moreno, R. et al. (2011a), 'Direct detection of the Enceladus water torus with Herschel', *A&A* **532**, L2.

Hartogh, P., Lis, D. C., Bockelée-Morvan, D. et al. (2011b), 'Ocean-like water in the Jupiter-family comet 103P/Hartley 2', *Nature* **478**(7368), 218–20.

Hendrix, A. R., Barth, C. A. and Hord, C. W. (1999), 'Ganymede's ozone-like absorber: observations by the Galileo ultraviolet spectrometer', *J. Geophys. Res.* **104**(E6), 14169–78.

Hodges Jr., R. R. and Johnson, F. S. [1968]. 'Lateral transport in planetary exospheres', *J. Geophys. Res. Space Phys.* 73(23), 7307–7317. DOI: https://doi.org/10.1029/JA073i023p07307.

Johnson, R. E. (1990), *Energetic Charged-Particle Interactions with Atmospheres and Surfaces*. Springer. DOI: https://doi.org/10.1007/978-3-642-48375-2.

Johnson, R. E. (1997), 'Polar "caps" on Ganymede and Io revisited', *Icarus* **128**(2), 469–71.

Johnson, R. E., Carlson, R. W., Cassidy, T. A. and Fama, M. (2013), 'Sputtering of Ices', in Gudipati, M., Castillo-Rogez, J. (eds.), *The Science of Solar System Ices*. Astrophysics and Space Science Library, vol. 356. DOI: https://doi.org/10.1007/978-1-4614-3076-6_17.

Johnson, R. E., Carlson, R. W., Cooper, J. F. et al. (2004), Radiation effects on the surfaces of the Galilean satellites, in Bagenal, F., Dowling, T. E. and McKinnon, W. B., eds., 'Jupiter: The Planet, Satellites and Magnetosphere', Cambridge University Press, pp. 485–512.

Johnson, R. E., Lanzerotti, L. J., Brown, W. L. and Armstrong, T. P. (1981), 'Erosion of Galilean satellite surfaces by Jovian magnetosphere particles', *Science* **212**(4498), 1027–30.

Johnson, R. E., Oza, A. V., Leblanc, F. et al. (2019), 'The origin and fate of O_2 in Europa's ice: an atmospheric perspective', *Space Sci. Rev.* **215**(1), 20.

Kanik, I., Johnson, P. V., Das, M. B., Khakoo, M. A. and Tayal, S. S. (2001), 'Electron-impact studies of atomic oxygen: I. Differential and integral cross sections; experiment and theory', *J. Phys. B: At. Mol. Opt. Phys.* **34**, 2647–65.

Kanik, I., Noren, C., Makarov, O. P. et al. (2003), 'Electron impact dissociative excitation of O_2: 2. Absolute emission cross sections of the OI(130.4 nm) and OI(135.6 nm) lines', *J. Geophys. Res.* **108**(E11), 5126.

Khurana, K. K., Pappalardo, R. T., Murphy, N. and Denk, T. (2007), 'The origin of Ganymede's polar caps', *Icarus* **191**(1), 193–202.

Kivelson, M. G., Bagenal, F., Kurth, W. S. et al. (2004), 'Magnetospheric interactions with satellites', in Bagenal, F., Dowling, T. E., and McKinnon, W. B., eds., *Jupiter: The Planet, Satellites and Magnetosphere*, Cambridge University Press, pp. 513–36.

Krimigis, S. M., Armstrong, T. P., Axford, W. I. et al. (1977), 'The Low Energy Charged Particle (LECP) experiment on the Voyager Spacecraft', *Space Sci. Rev.* **21**(3), 329–54.

Langevin, Y., Piccioni, G., Filacchione, G., Poulet, F. and Dumesnil, C. (2018), 'MAJIS, the VIS-IR imaging spectrometer of JUICE', in *IPM 2018, International Workshop on Instrumentation for Planetary Missions, Technische Universität Berlin*, p. E1. https://ui.adsabs.harvard.edu/abs/2018ipm..confE...1L

Lanzerotti, L. J., Brown, W. L., Poate, J. M. and Augustyniak, W. M. (1978), 'On the contribution of water products from Galilean satellites to the Jovian magnetosphere', *Geophys. Res. Lett.* **5**(2), 155–8.

Leblanc, F., Oza, A. V., Leclercq, L. et al. (2017), 'On the orbital variability of Ganymede's atmosphere', *Icarus* **293**, 185–98.

Liuzzo, L., Poppe, A. R., Paranicas, C. et al. (2020), 'Variability in the energetic electron bombardment of Ganymede', *J. Geophys. Res.* **125**(9), e28347.

Makarov, O. P., Ajello, J. M., Vatti Palle, P. et al. (2004), 'Kinetic energy distributions and line profile measurements of dissociation products of water upon electron impact', *J. Geophys. Res.* **109**(A18), 9303.

Marconi, M. L. (2007), 'A kinetic model of Ganymede's atmosphere', *Icarus* **190**, 155–74.

McGrath, M. A., Jia, X., Retherford, K. et al. (2013), 'Aurora on Ganymede', *J. Geophys. Res.* **118**, 2043–54.

McGrath, M. A., Lellouch, E., Strobel, D. F., Feldman, P. D. and Johnson, R. E. (2004), Satellite atmospheres, *in* Bagenal, F., Dowling, T. E., and McKinnon, W. B., eds., *Jupiter: The Planet, Satellites and Magnetosphere*, Cambridge University Press, pp. 457–83.

Molyneux, P. M., Nichols, J. D., Bannister, N. P. et al. (2018), 'Hubble Space Telescope observations of variations in Ganymede's oxygen atmosphere and aurora', *J. Geophys. Res.* **123**(5), 3777–93.

Moore, J. M., Chapman, C. R., Bierhaus, E. B. et al. (2004), Callisto, in F. Bagenal, T. E. Dowling and W. B. McKinnon, eds., *Jupiter: The Planet, Satellites and Magnetosphere*, Cambridge University Press, pp. 397–426.

Musacchio, F., Saur, J., Roth, L. et al. (2017), 'Morphology of Ganymede's FUV auroral ovals', *J. Geophys. Res.* **122**(3), 2855–76.

Noll, K. S., Johnson, R. E., Lane, A. L., Domingue, D. L. and Weaver, H. A. (1996), 'Detection of ozone on Ganymede', *Science* **273**(5273), 341–3.

Orton, G. S., Spencer, J. R., Travis, L. D., Martin, T. Z. and Tamppari, L. K. (1996), 'Galileo photopolarimeter-radiometer observations of Jupiter and the Galilean satellites', *Science* **274**(5286), 389–91.

Oza, A. (2017), Detection and dynamics of satellite exospheres, Thesis, Université Pierre et Marie Curie – Paris VI. https://tel.archives-ouvertes.fr/tel-01687043.

Oza, A. V., Johnson, R. E. and Leblanc, F. (2018), 'Dusk/dawn atmospheric asymmetries on tidally-locked satellites: O_2 at Europa', *Icarus* **305**, 50–5.

Oza, A. V., Leblanc, F., Johnson, R. E. et al. (2019), 'Dusk over dawn O_2 asymmetry in Europa's near-surface atmosphere', *Planet. Space Sci.* **167**, 23–32.

Pappalardo, R. T., Collins, G. C., Head, J. W. et al. (2004), Geology of Ganymede, in F. Bagenal, T. E. Dowling and W. B. McKinnon, eds., *Jupiter: The Planet, Satellites and Magnetosphere*, Vol. 1, pp. 363–96.

Piccioni, G., Tommasi, L., Langevin, Y. et al. (2019), Scientific goals and technical challenges of the MAJIS imaging spectrometer for the JUICE mission, in '2019 IEEE 5th International Workshop on Metrology for AeroSpace (MetroAeroSpace)', IEEE, pp. 318–23.

Plainaki, C., Massetti, S., Jia, X. et al. (2020a), 'Kinetic simulations of the Jovian energetic ion circulation around Ganymede', *ApJ* **900**(1), 74.

Plainaki, C., Milillo, A., Massetti, S. et al. and Rispoli, R. (2015), 'The H_2O and O_2 exospheres of Ganymede: the result of a complex interaction between the Jovian magnetospheric ions and the icy moon', *Icarus* **245**, 306–19.

Plainaki, C., Sindoni, G., Grassi, D. et al. (2020b), 'Preliminary estimation of the detection possibilities of Ganymede's water vapor environment with MAJIS', *Planet. Space Sci.* **191**, 105004.

Poppe, A. R., Fatemi, S. and Khurana, K. K. (2018), 'Thermal and energetic ion dynamics in Ganymede's magnetosphere', *J. Geophys. Res.* **123**(6), 4614–637.

Rezac, L., Zhao, Y., Hartogh, P. et al. (2019), 'Three-dimensional analysis of spatial resolution of MIRO/Rosetta measurements at 67P/Churyumov-Gersimenko', *A&A* **630**, A34.

Roth, L. (2021), 'A stable H_2O atmosphere on Europa's trailing hemisphere from HST images', *Geophys. Res. Lett.* 48(20), e2021GL094289. DOI: https://doi.org/10.1029/2021GL094289.

Roth, L., Ivchenko, N., Gladstone, G. R. et al. (2021), 'A sublimated water atmosphere on Ganymede detected from Hubble Space Telescope observations', *Nat. Astron.* **5**, 1043–51. DOI: https://doi.org/10.1038/s41550-021-01426-9.

Roth, L., Saur, J., Retherford, K. D. et al. (2014), 'Transient water vapor at Europa's south pole', *Science* **343**(6167), 171–4.

Roth, L., Saur, J., Retherford, K. D. et al. (2016), 'Europa's far ultraviolet oxygen aurora from a comprehensive set of HST observations', *J. Geophys. Res.* **121**, 2143–70.

Saur, J., Duling, S., Roth, L. et al. (2015), 'The search for a subsurface ocean in Ganymede with Hubble Space Telescope observations of its auroral ovals', *J. Geophys. Res.* **120**, 1715–37.

Saur, J., Strobel, D. F. and Neubauer, F. M. (1998), 'Interaction of the Jovian magnetosphere with Europa: constraints on the neutral atmosphere', *J. Geophys. Res.* **103**(E9), 19947–62.

Shematovich, V. I. (2016), 'Neutral atmosphere near the icy surface of Jupiter's moon Ganymede', *Sol. Syst. Res.* **50**(4), 262–80.

Shi, M., Baragiola, R. A., Grosjean, D. E. et al. (1995), 'Sputtering of water ice surfaces and the production of extended neutral atmospheres', *J. Geophys. Res.* **100**(E12), 26387–96.

Smith, H. T., Mitchell, D. G., Johnson, R. E., Mauk, B. H. and Smith, J. E. (2019), 'Europa neutral torus confirmation and characterization based on observations and modeling', *ApJ* **871**(1), 69.

Smyth, W. H. and Marconi, M. L. (2006), 'Europa's atmosphere, gas tori, and magnetospheric implications', *Icarus* **181**, 510–26.

Spencer, J. R. (1987), 'Icy Galilean satellite reflectance spectra: less ice on Ganymede and Callisto?', *Icarus* **70**(1), 99–110.

Spencer, J. R., Calvin, W. M. and Person, M. J. (1995), 'CCD spectra of the Galilean satellites: molecular oxygen on Ganymede', *J. Geophys. Res.* **100**(E9), 19049–56.

Spencer, J. R., Lebofsky, L. A. and Sykes, M. V. (1989), 'Systematic biases in radiometric diameter determinations', *Icarus* **78**(2), 337–54.

Stern, S. A., Slater, D. C., Scherrer, J. et al. (2008), 'ALICE: the ultraviolet imaging spectrograph aboard the New Horizons Pluto-Kuiper Belt Mission', *Space Sci. Rev.* **140**(1–4), 155–87.

Strobel, D. F., Saur, J., Feldman, P. D. and McGrath, M. A. (2002), 'Hubble Space Telescope space telescope imaging spectrograph search for an atmosphere on Callisto: a Jovian unipolar inductor', *Astrophys. J.* **581**, L51–L54.

Taylor, G. E. (1971), 'Occultation of Beta Scorpii C by Io on May 14, 1971', *Nature* **234**(5329), 405–6.

Teolis, B. D., Plainaki, C., Cassidy, T. A. and Raut, U. (2017), 'Water ice radiolytic O_2, H_2, and H_2O_2 yields for any projectile species, energy, or temperature: a model for icy astrophysical bodies', *J. Geophys. Res.* **122**(10), 1996–2012.

Teolis, B. D., and Waite, J. H. [2016], 'Dione and Rhea seasonal exospheres revealed by Cassini CAPS and INMS', *Icarus* **272**, 277–89. DOI: https://doi.org/10.1016/j.icarus.2016.02.031.

Turc, L., Leclercq, L., Leblanc, F., Modolo, R. and Chaufray, J. Y. (2014), 'Modelling Ganymede's neutral environment: a 3D test-particle simulation', *Icarus* **229**, 157–169.

Vorburger, A., Fatemi, S., Galli, A. et al. (2022), '3D Monte-Carlo simulation of Ganymede's water exosphere', *Icarus* **375**, 114810. DOI: https://doi.org/10.1016/j.icarus.2021.114810.

Wirström, E. S., Bjerkeli, P., Rezac, L., Brinch, C. and Hartogh, P. (2020), 'Effect of the 3D distribution on water observations made with the SWI. I. Ganymede', *A&A* **637**, A90.

Wood, J. A. (1957), 'Sputtering and the drag coefficient in the regime of free molecular flow', *AJ* **62**, 40.

Yamada, T., Rezac, L., Larsson, R. et al. (2018), 'Solving non-LTE problems in rotational transitions using the Gauss–Seidel method and its implementation in the Atmospheric Radiative Transfer Simulator', *A&A* **619**, A181.

Yung, Y. L. and McElroy, M. B. (1977), 'Stability of an oxygen atmosphere on Ganymede', *Icarus* **30**(1), 97–103.